

論文 / 著書情報
Article / Book Information

論題(和文)	
Title(English)	Intensity Difference Map (IDM) Accuracy Analysis for OPC Efficiency Verification and Further Enhancement
著者(和文)	AWAD Ahmed, 高橋篤司, 田中聡, 児玉親亮
Authors(English)	Ahmed Awad, Atsushi Takahashi, Satoshi Tanaka, Chikaaki Kodama
出典(和文)	, Vol. 10, , pp. 28-38
Citation(English)	IPSJ Trans. on System LSI Design Methodology, Vol. 10, , pp. 28-38
発行日 / Pub. date	2017, 2
権利情報 / Copyright	<p>ここに掲載した著作物の利用に関する注意: 本著作物の著作権は(社)情報処理学会に帰属します。本著作物は著作権者である情報処理学会の許可のもとに掲載するものです。ご利用に当たっては「著作権法」ならびに「情報処理学会倫理綱領」に従うことをお願いいたします。</p> <p>The copyright of this material is retained by the Information Processing Society of Japan (IPSJ). This material is published on this web site with the agreement of the author (s) and the IPSJ. Please be complied with Copyright Law of Japan and the Code of Ethics of the IPSJ if any users wish to reproduce, make derivative work, distribute or make available to the public any part or whole thereof.</p>

Intensity Difference Map (IDM) Accuracy Analysis for OPC Efficiency Verification and Further Enhancement

AHMED AWAD^{1,a)} ATSUSHI TAKAHASHI^{1,b)} SATOSHI TANAKA^{2,c)} CHIKAACHI KODAMA^{2,d)}

Received: June 1, 2016, Revised: September 5, 2016,
Accepted: October 19, 2016

Abstract: Optical Proximity Correction (OPC) is still nominated as a main stream in printing Sub-16 nm technology nodes in optical micro-lithography. However, long computation time is required to generate mask solutions with acceptable wafer image quality. Intensity Difference Map (IDM) has been recently proposed as a fast methodology to shorten OPC computation time with preserving acceptable wafer image quality. However, IDM has been evaluated only under a relatively relaxed Edge Placement Error (EPE) constraint of the final mask solution. Such an evaluation does not provide a satisfactory confirmation of the effectiveness of IDM if strict EPE constraints are imposed. In this paper, the accuracy of IDM is deeply analyzed to confirm its validity in terms of wafer image estimation accuracy along with its efficiency in shortening computation time. Thereafter, the stability of IDM accuracy against the increase in pattern area/density is confirmed. Finally, the regions suffering from lack of accuracy are analyzed for further enhancement. Experimental results show that congestion in the mask pattern forms a cardinal source of the lack of accuracy which is compensated through optimized selection of the kernels included in IDM.

Keywords: Optical Proximity Correction (OPC), Intensity Difference Map (IDM), Root Mean Square Error (RMSE), absolute intensity error, Kernel Band (K-band) area

1. Introduction

As advanced technology nodes continue scaling down into sub-16 nm regime, the industry relies heavily on Resolution Enhancement Techniques (RETs) to preserve acceptable wafer image quality onto the silicon wafer. Optical Proximity Correction (OPC) is dominant among RETs in the current 193 nm immersion lithography since Next Generation Lithography (NGL) is still not practically ready [1], [2].

In the field of OPC, a mask pattern is iteratively adjusted followed by wafer image computation following some mathematical models. The computed wafer image is compared with the target pattern to either determine algorithm termination with outputting satisfactory mask solution or guide the next OPC iteration adjustments [3]. **Figure 1** illustrates the general scheme of OPC.

A great effort is evident in the field of OPC both in the literature and commercial OPC tools [4], [5], [6]. However, the required OPC computation time to find a final mask solution becomes a crucial factor in the industry. For example, an OPC used in metal layers can run into 3-5 days for realistic industrial cases. Even for simplified unidirectional layers in the poly-silicon, OPC might take 24 hours to find the final mask solution [7]. However, the trade-off between wafer image quality and computation

time is often pushed in favor of preserving acceptable image quality with sacrificing the need for shortening the computation time. This results in abrupt increase in the turnaround time of chip production.

Wafer image computation is the principal contributor for the total OPC computation time. Wafer image is often simulated using a lithographic model which consists of optical model and resist model. Wafer image computation accuracy plays a dominant role in the quality of the OPCed mask solution since the computed image typically guides the next OPC response [8]. However, there is a trade-off between wafer image computation time and wafer image estimation accuracy. This trade-off is often pushed in favor of maximizing the estimation accuracy of the wafer image to ensure proper OPC response.

Intensity Difference Map (IDM) has been recently published within our OPC framework in Ref. [9] as a methodology to speedup wafer image computation with preserving acceptable wafer image estimation accuracy. In IDM, the wafer image of a given mask is estimated through the intensity information utilized from some reference mask. These information are exploited to compensate a roughly estimated wafer image of the mask of interest within a short computation time.

Selection of an appropriate reference mask results in better overall intensity estimation. While our work in Ref. [9] suggests using target pattern as reference mask, an initially OPCed mask solution has been suggested to be the reference mask for better estimation accuracy in our work proposed in Ref. [10].

Adaptation of IDM has been proposed in our work in Ref. [11], wherein, the IDM is iteratively corrected following the local mask density difference between the mask of interest and the refer-

¹ Department of Communications and Computer Engineering, Graduate School of Science and Engineering, Tokyo Institute of Technology, Meguro, Tokyo 152–8550, Japan

² Toshiba Corporation Storage & Electronic Devices Solutions Company, Yokohama, Kanagawa 247–8585, Japan

^{a)} awad.ahmed@eda.ce.titech.ac.jp

^{b)} atsushi@eda.ce.titech.ac.jp

^{c)} satoshi2.tanaka@toshiba.co.jp

^{d)} chikaaki1.kodama@toshiba.co.jp

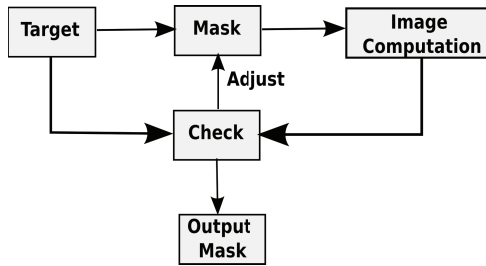


Fig. 1 OPC scheme.

ence mask, for more accurate estimation. This work has been expanded to consider process variation in our work in Ref. [12].

In the previous work in Refs. [9], [10], [11], [12], IDM methodology has been evaluated in terms of wafer image quality of the output OPCed mask solution under relatively relaxed Edge Placement Error (EPE) constraints. A deep investigation of the intensity estimation error has not been performed. Thus, mask solutions might not be qualitatively sufficient if strict EPE constraints are imposed. Additionally, such evaluation might not be sufficient to confirm the validity of IDM methodology for very complicated resist models. Furthermore, the stability of IDM methodology with the increased area/density of patterns has not been verified as well.

In this paper, we deeply analyze the accuracy of IDM during OPC to confirm its usability if strict EPE constraints are requested by the industry. This is achieved through introducing a set of parameters that measure both intensity and wafer image estimation errors. Thereafter, the stability of IDM methodology is confirmed through analyzing the intensity/image accuracy metrics with pattern area/density increase. Finally, analyzing the regions suffering from lack of accuracy is proposed followed by suggestions for further enhancements. Our contributions are summarized as follows:

- The accuracy of IDM is confirmed in terms of intensity estimation through deep analysis for the intensity of a set of tap points defined on the target boundary in each OPC iteration using maximum absolute intensity error and Root Mean Square Error (RMSE) between the estimated and exact intensity values of the tap points.
- The accuracy of IDM is confirmed in terms of wafer image estimation through analyzing the maximum line width of the XOR region between both the golden (exact) wafer image and estimated wafer image using IDM.
- The stability of IDM is verified through confirming that IDM preserves stable intensity/image accuracy with pattern area and density increase.
- The regions suffering from lack of accuracy are analyzed, wherein, congestion in the pattern has been found as a cardinal source for such loss of accuracy.
- Suggestions to improve the accuracy of IDM methodology are proposed. This includes: compensating this loss through gradually expanding the set of kernels included in IDM to satisfy the required accuracy, and sub-regions convolutions.

The rest of this paper is organized as follows: Section 2 describes previous work related to shortening OPC computation time. Section 3 describes lithographic terminology and IDM

methodology. Section 4 proposes IDM efficiency analysis in terms of wafer image accuracy, computation time reduction, and stability. Section 5 discusses adaptation of IDM and its impact on the overall estimation accuracy. Section 6 defines the regions potential to suffer from lack of accuracy followed by discussing possible enhancements of IDM accuracy. Finally, Section 7 concludes this paper.

2. Previous Work

Large body of work has been dedicated to improve wafer image quality in OPC, such as assisting features insertion [13], [14], moving fragmented edges [15], [16], [17], and Inverse Lithography Technology (ILT) [18], [19]. However, shortening computation time constraint has been often relaxed in most of the OPC algorithms since there is no tolerance to compromise quality for speed from circuit functionality perspective. However, the huge computation time needed to find a mask solution for advanced technology nodes increases the need for fast and accurate algorithms by the industry.

To accelerate OPC computation time, several algorithms have been proposed in the literature to reduce wafer image computation time. A linearized model to estimate the intensity per pixel has been proposed in Ref. [20] at the cost of accuracy loss. A fast printability verification method has been proposed in Ref. [21], wherein, some regions are tagged as critical since they suffer from large image distortions onto the wafer. The intensity of such critical regions is accurately estimated. On the other hand, the intensity of non-critical regions is roughly estimated within a short time. However, the computation time for such an algorithm is expected to dramatically increase for advanced technology nodes, wherein, distortions are widely distributed within the layout region. Under the assumption that intensity follows the normal distribution, Process Variation OPC (PV-OPC) algorithm estimates the intensity within a short computation time [7]. Mask Optimization Solution With Process Window Aware Inverse Correction (MOSAIC) algorithm proposed a relatively fast ILT methodology with some loss of accuracy [22].

Intensity Difference Map (IDM) has been recently introduced in our work in Refs. [9], [10] as a fast methodology to estimate the wafer image for a given mask using some reference mask. Adaptive version of IDM has been proposed as well in our work in Refs. [11], [12]. However, the performance of IDM has been only verified through evaluating the final OPCed mask solutions outputted from including IDM in the OPC recipe under relatively relaxed EPE constraint. Such an evaluation is not sufficient to ensure the usability of IDM for realistic industrial cases along with its stability against the increasing pattern area/density.

3. Lithographic Terminology and Intensity Difference Map (IDM) Methodology

3.1 Pattern Terminology

Let R be a region of pixels. Let T be a target pattern defined in the layout region such that $T \subseteq R$. Similarly, let M denote a mask defined in R such that $M \subseteq R$. Both the target and the mask consist of a number of a non-overlapped rectilinear polygons where a polygon consists of a set of connected pixels. Let

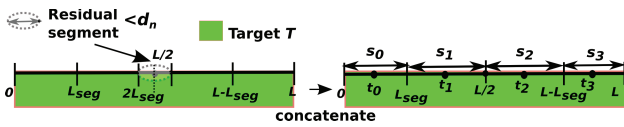
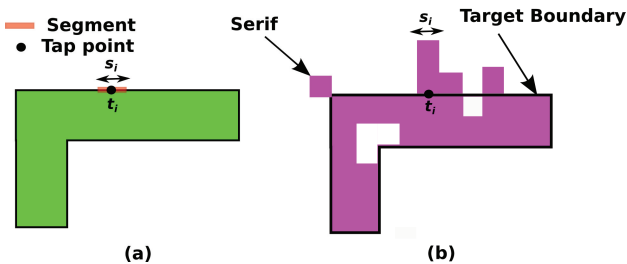

 Fig. 2 Fragmentation process for L pixels edge in the target boundary.


Fig. 3 (a) Target pattern. (b) OPCed mask.

S be a polygon. If a pixel p is contained in S , it is denoted by $p \in S$. Furthermore, if $p \in S \in T$, it is simply denoted by $p \in T$. Similarly, if $p \in S \in M$, it is denoted by $p \in M$.

Target boundary is fragmented into segments which move orthogonal to the target boundary during OPC. Segments are aligned from both corners towards the center of a target edge with user-defined segment length. Segment length, denoted by L_{seg} , is assumed be greater than or equal to the minimum allowable mask notch width, denoted by d_n , to satisfy mask notch design rule during segment movement for realistic industrial applications. Additionally, if a segment length is less than d_n , it is concatenated with its neighbors to satisfy mask notch rule. **Figure 2** illustrates the fragmentation process used in this paper where s_i denotes an arbitrary segment. Notice that, target boundary is fragmented into segments in initialization stage prior to OPC. Thereafter, those segments keep their fixed length while moving orthogonal to their target edges during the iterative OPC process. However, more effective fragmentation techniques (such as adaptive segment refinement [7]) will be integrated in our OPC methodology in the future to generate higher quality mask solutions.

The center of each segment on the target boundary is defined as a tap point (as shown in Fig. 2) whose intensity is included in the OPC recipe to determine the shifting distance/direction of the segments. Let t_i denote the tap point of segment s_i and A denote the set of tap points defined along the target boundary.

Unprintable squared features (serifs) are exploited as well to improve wafer image quality. **Figure 3** illustrates a target pattern and its OPCed mask.

3.2 Lithographic Model

In this paper, Sum of Coherent Systems (SOCS) model is used to represent the intensity map (aerial image) through a mask in region R . This map represents the distribution of light intensity in the wafer plane. In SOCS model, optical system is decomposed into a set of coherent kernels working as low pass filters. Each kernel has an eigenfunction represents its filtering behavior and eigenvalue which represents its weight for intensity estimation [23]. For a mask M , intensity value in pixel p using set of kernels K , denoted by $I(M, K, p)$, is given in Eq. (1) wherein, σ_k and $\phi_k(p)$ represent the eigenvalue and the eigenfunction for kernel $k \in K$ in pixel p , respectively, and \otimes denotes convolution

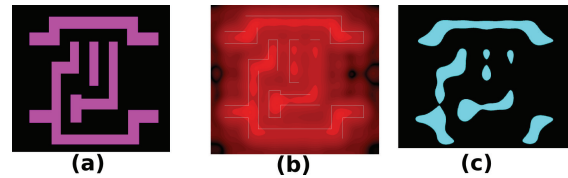


Fig. 4 (a) Mask pattern. (b) Intensity map. (c) Wafer image.

operation.

$$I(M, K, p) = \sum_{k \in K} \sigma_k |(\phi_k(p) \otimes M)|^2 \quad (1)$$

A higher weight kernel has more contribution in intensity value than a lower weight kernel. The more kernels usage, the more coverage of diffraction angles in the optical system which turns out into better estimation accuracy of the intensity map. However, computation time increases with kernels number due to the computationally expensive convolutions.

Resist model aims to reflect the resist exposure response upon the projection of light intensity on the resist regions. In this paper, a simple Constant Threshold Resist (CTR) model is utilized through predefining intensity threshold of exposure I_{th} . In this model, if a pixel intensity is greater than I_{th} , the resist is exposed and removed. Otherwise, the resist remains after patterning. $G(M, K, p)$ represents the wafer image function following this CTR model using set of kernels K in pixel p which is formulated in Eq. (2). Notice that, for realistic industrial cases, a generalized formulation of CTR model is exploited, wherein, Gaussian kernel is included in wafer image computation [24], [25], [26]. For advanced technology nodes, more complicated resist models, such as, Variable Threshold Resist (VTR) might be required [27].

$$G(M, K, p) = \begin{cases} 1; & I(M, K, p) \geq I_{th} \\ 0; & \text{Otherwise} \end{cases} \quad (2)$$

Figure 4 (b) illustrates an intensity map of the mask shown in Fig. 4 (a) and Fig. 4 (c) illustrates the obtained wafer image for that mask after applying CTR model for all pixels in the region.

3.3 Intensity Difference Map (IDM) Methodology

Intensity Difference Map (IDM) is the difference between two intensity maps estimated using different sets of SOCS kernels. Let K and K' be two sets of kernels such that $K' \subset K$, IDM of mask M between K and K' in pixel p , denoted by $I_{diff}(M, K, K', p)$, is given in Eq. (3). **Figure 5** illustrates IDM for a given mask between all kernels K and top weight kernel $k_0 \in K$.

$$I_{diff}(M, K, K', p) = I(M, K, p) - I(M, K', p) \quad (3)$$

As mentioned in Ref. [21], the relative contribution of a kernel in intensity value decays with going towards lower weight kernels. Based on our observation, during OPC, the degree of change in the intensity at certain pixel is relatively small if estimated using lower weight kernels. On the other hand, this change in intensity is significant if estimated using the top weight kernel whose relative contribution in intensity estimation is dominant. For example, if the top weight kernel contributes by around 60% from the overall intensity value at certain pixel, the degree of change

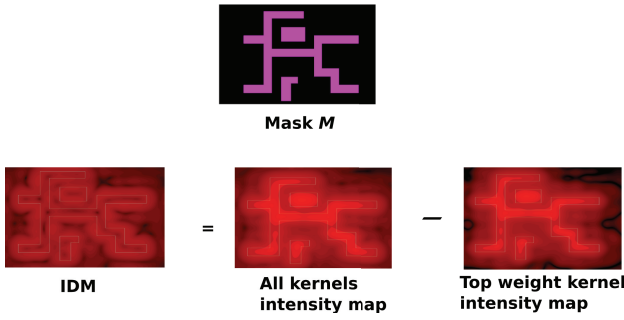


Fig. 5 IDM between all kernels and top weight kernel for a given mask M .

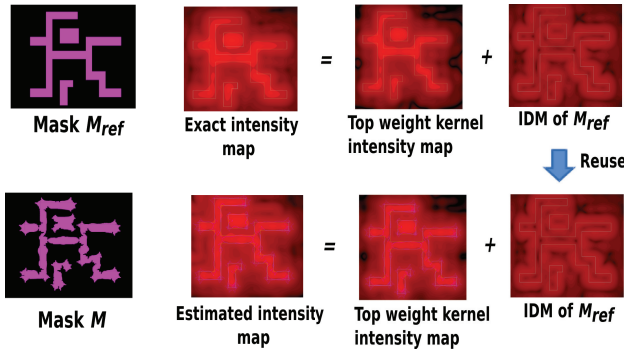


Fig. 6 IDM methodology to estimate the intensity map of mask M using the IDM constructed from reference mask M_{ref} .

in that pixel intensity during OPC iterations might reach around 10% if estimated using top weight kernel while this change might not exceed 5% for the other lower weight kernels.

Therefore, IDM between all kernels and top weight kernel has been exploited to accelerate intensity map computation following the observation that lower weight kernels contribution in intensity value is almost invariant of mask shape slight changes. In our work published in Ref. [9], IDM is constructed from some reference mask M_{ref} of a target pattern T . The intensity through mask M for the same target is roughly estimated in a pixel p using only the top weight kernel. The resultant roughly estimated intensity is then compensated by adding IDM as given in Eq. (4) where K represents the set of all kernels and $k_0 \in K$ represents the top weight kernel. The superscript $*$ implies an estimation of the intensity. This turns out into estimating the intensity map with just one convolution per OPC iteration. Figure 6 illustrates this IDM methodology in OPC with using target pattern as M_{ref} .

$$I^*(M, K, p) = I(M, \{k_0\}, p) + I_{diff}(M_{ref}, K, \{k_0\}, p) \quad (4)$$

As target pattern is often unprintable around its boundaries, the intensity information that IDM entails around those boundaries suffer from lack of accuracy if T is used as reference mask. Thus, our work in Ref. [10] suggests to apply one extra OPC step on T to generate an initial mask solution $M^{[0]}$ whose IDM is constructed to work as a static compensative map during OPC. Thus, the intensity of mask M is estimated as in Eq. (4) with setting M_{ref} to $M^{[0]}$. In this paper, static IDM refers to IDM with using $M^{[0]}$ as reference mask.

4. Intensity Difference Map (IDM) Methodology Efficiency Analysis and Verification

This section proposes a deep analysis to verify the efficiency

of IDM. First of all, IDM improvement on intensity and wafer image estimation accuracy is confirmed. Then, IDM efficiency in shortening wafer image computation time is verified. Finally, the stability of IDM methodology is verified.

All plots were obtained using Lithosim simulator from IC-CAD 2013 CAD contest which uses industrial optical models with 193 nm wavelength. In Lithosim, layout region is defined in 1024×1024 pixels where each pixel represents $1 \text{ nm} \times 1 \text{ nm}$. The total set of kernels in Lithosim is $K = \{k_0, k_1, \dots, k_{23}\}$ where k_0 is the top weight kernel. CTR model is used to simulate the wafer image with $I_{th} = 0.225$. The testing benchmarks used for analysis are the ones released by IBM for the contest which represent the most challenging M1 patterns for 32 nm technology nodes [28]. Shifting and hammering modules in the OPC algorithm published in Ref. [9] are used in our analysis.

4.1 Wafer Image Estimation Accuracy Evaluation

Let $I(M, K, p)$ denote the exact (golden) intensity in pixel p simulated using all kernels K in the lithographic system and let $I^*(M, K, p)$ denote an estimated intensity using some estimation model. Estimated wafer image in pixel p , denoted by $G^*(M, K, p)$, is the image extracted from the estimated intensity map $I^*(M, K, p)$ with applying a resist model (CTR in this paper).

4.1.1 Evaluation Metrics

Tap points defined along the target boundary typically have big loss of accuracy in intensity estimation due to the high frequencies located around them in the spatial domain. Thus, for wafer image estimation accuracy, we define three metrics as follows:

- (1) **Absolute Intensity Error:** The absolute difference between golden intensity and the estimated intensity for a given tap point t as given in Eq. (5). Maximum absolute error among the set of tap points in the target pattern forms a key parameter for accuracy evaluation since its high values result into significant misleading of the OPC response. Let E_{max} denote the maximum absolute intensity error for a mask M as given in Eq. (6), where A denotes the set of tap points defined.

$$E(M, t) = |I(M, K, t) - I^*(M, K, t)| \quad (5)$$

$$E_{max}(M) = \max_{t \in A} \{E(M, t)\} \quad (6)$$

- (2) **Intensity Root Mean Square Error (IRMSE):** The sample standard deviation of the differences between exact intensity and estimated intensity. The sample of interest is the set of tap points defined. Thus, IRMSE is formulated as given in Eq. (7) where A denotes the set of tap points. Higher IRMSE values indicate less accurate estimation.

$$IRMSE = \sqrt{\frac{1}{|A|} \sum_{t \in A} (I(M, K, t) - I^*(M, K, t))^2} \quad (7)$$

- (3) **Maximum Kernel band (K-band) Line Width:** Kernel band (K-band) area is defined as the area of XORing both golden and estimated images as given in Eq. (8). Figure 7 illustrates the K-band for a given mask pattern between exact wafer image and estimated wafer image using only top weight kernel.

$$KB(M) = |\{p \in R \mid G(M, K, p) \oplus G^*(M, K, p) = 1\}| \quad (8)$$

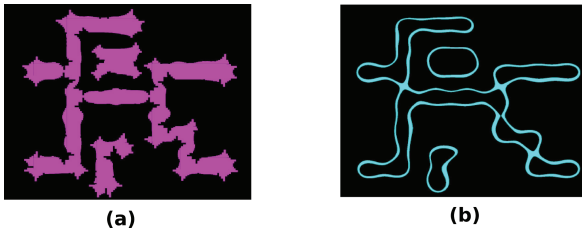


Fig. 7 (a) Mask pattern. (b) K-band between exact wafer image and the image simulated using only top weight kernel.

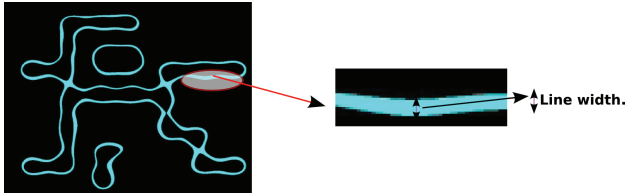


Fig. 8 K-band line width.

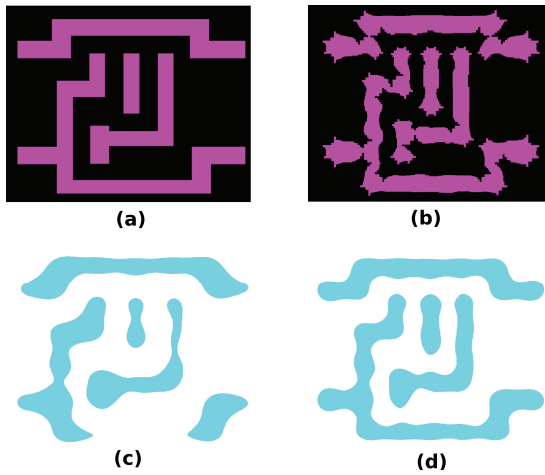


Fig. 9 (a) Target pattern. (b) Mask solution. (c) Wafer image when using target as the mask. (d) Wafer image when using the mask solution.

K-band line width is defined as the length of the line orthogonal to the target boundary which connects the starting and ending points of the K-band at some point on T as illustrated in Fig. 8. The maximum line width in the layout is important metric in twofolds: (1) A thick K-band line width indicates a large loss of accuracy. (2) If the maximum K-band line width exceeds the maximum allowable EPE, it indicates that the wafer image estimation methodology fails to preserve acceptable wafer image quality and including it in the OPC recipe is risky as it might yield into mask solutions with circuit malfunctions.

4.1.2 Case of Study

Lets consider the target pattern shown in Fig. 9(a), shifting (with 10 nm segment length) and hammering modules of the OPC algorithm published in Ref. [9] were applied on this target with exploiting static IDM for intensity estimation during OPC. The final mask solution is shown in Fig. 9(b) with its wafer image shown in Fig. 9(d). The maximum allowable EPE is assumed to be 15 nm following ICCAD 2013 CAD contest evaluation. The total number of tap points in this test-case optimization is 952.

To evaluate the accuracy of IDM methodology for different masks, the resultant mask solution from each OPC iteration has been analyzed for intensity/image estimation accuracy. That is, in

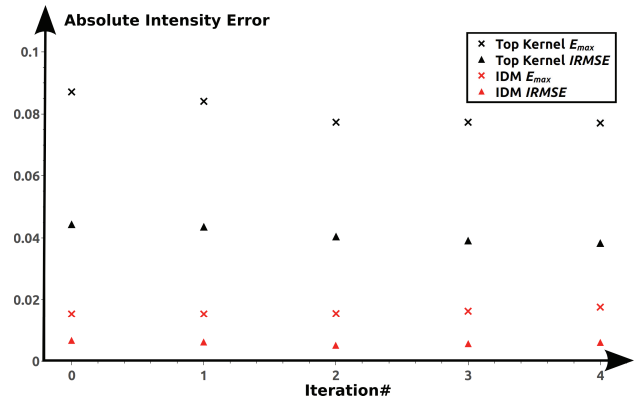


Fig. 10 Maximum absolute intensity error and IRMSE for the mask generated during each iteration when applying OPC on the target shown in Fig. 9(a). Intensity has been estimated using only top weight kernel and top weight kernel compensated with static IDM.

each iteration, the OPCed mask intensity map is simulated using all kernels (golden intensity map), using only top weight kernel, and using top weight kernel compensated with static IDM. CTR model is then applied to extract the wafer image for each case. Note that, this evaluation is independent of the way by which the mask solution is found. Thus, either using static IDM, or golden intensity map to guide the OPC response would not impact the evaluation for this case of study as the mask outputted from each iteration is evaluated.

Figure 10 illustrates the maximum absolute intensity error and IRMSE among tap points for each mask (outputted from each iteration) using only top weight kernel and using compensation with static IDM. The maximum absolute error has been effectively reduced by 77%. This shows that IDM effectively accumulates the maximum loss of accuracy which guarantees proper OPC response for the inputted intensity. IRMSE has been effectively reduced by more than 75%. This indicates the minimization of the deviation of estimated intensity values from the exact intensity values. Thus, IDM effectively accumulates the loss of accuracy in intensity estimation of the mask pattern. Notice that IRMSE and the maximum intensity estimation error with IDM compensation (which are resultant from the lower weight kernels since top weight kernel intensity is exactly obtained by simulation) keep small values which do not exceed 8% of the threshold intensity of exposure in the worst case, regardless to the mask changes during OPC iterations. This provides an empirical proof of our insight for IDM invariance against mask shape slight changes during OPC.

Figure 11 illustrates the maximum line width of the K-band for each mask during each OPC. While the maximum line width when using only top weight kernel might reach 40 nm in its worst case, IDM compensation results in less than 6 nm maximum K-band line width which is almost one-third the maximum allowable EPE (15 nm). This shows the that IDM is capable of guiding the OPC response without significant wafer image quality degradation.

Figure 12 illustrates the K-band for the mask solution shown in Fig. 9(b). This includes the K-band between golden wafer image and the estimated wafer image using top weight kernel (shown in Fig. 12(a)), and the K-band between golden wafer image and

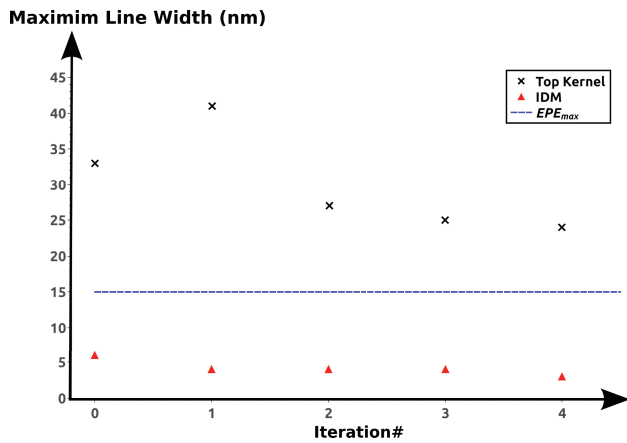


Fig. 11 Maximum K-band line width analysis during the OPC of the benchmark shown in Fig. 9 with 952 tap points number. EPE_{max} denotes the maximum allowable EPE which is 15 nm in this example.

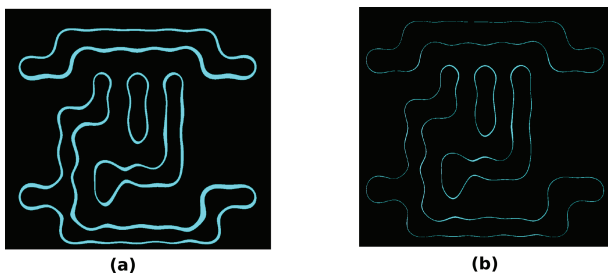


Fig. 12 K-band: (a) K-band between golden wafer image and wafer image estimated using only top weight kernel ($KB = 89382 \text{ nm}^2$). (b) K-band between golden wafer image and wafer image estimated with static IDM compensation ($KB = 16713 \text{ nm}^2$).

the estimated with static IDM (shown in Fig. 12 (b)). IDM compensation has achieved almost 82% reduction in the overall K-band area which demonstrates an evidence of the feasibility of this approach in reducing the overall K-band area, not only the maximum K-band line width.

4.2 Wafer Image Computation Time Evaluation

The main purpose of IDM is to accelerate wafer image computation, and thus, overall OPC computation time. Therefore, wafer image computation time has been analyzed for the case of study shown in Fig. 9.

Figure 13 illustrates wafer image computation time for each mask during OPC. This includes: exact wafer image computation and the estimated wafer image using IDM. With preserving acceptable estimation accuracy (as proven before), computation time has been effectively reduced by 91% from golden wafer image computation to the proposed estimation using static IDM. The reason is that, only one convolution operation is performed per iteration.

4.3 IDM Methodology Stability Evaluation

The purpose of IDM stability evaluation is to verify that IDM does a well compensation for intensity estimation for large scale patterns, wherein, patterns are densely/sparsely distributed among the entire layout region, not only in the region center. Such verification confirms that IDM methodology guarantees a fast OPC with acceptable quality for a full chip with complex patterns.

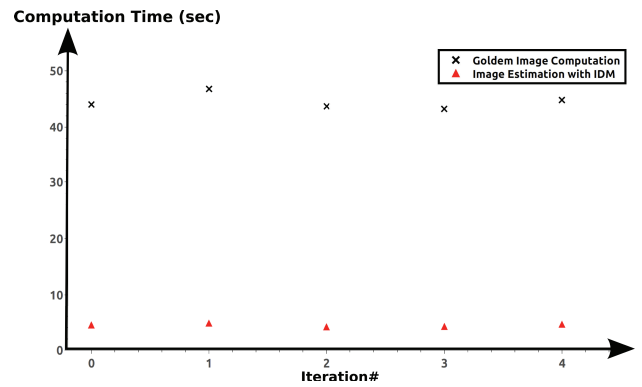


Fig. 13 Wafer image computation time analysis for OPC of the benchmark shown in Fig. 9.

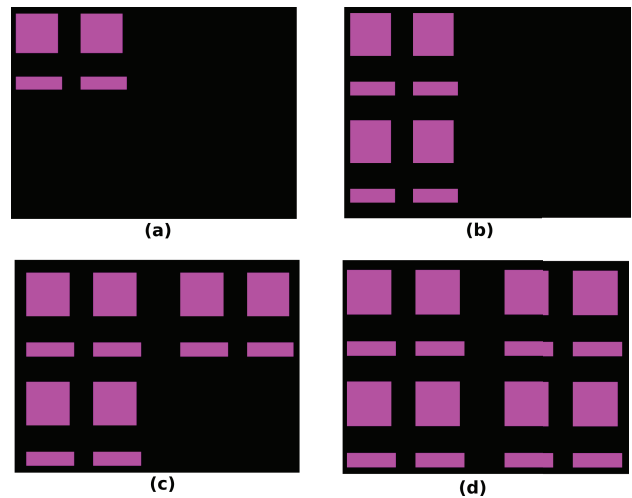


Fig. 14 Target patterns with different area/density: (a) Test-case 1. (b) Test-case 2. (c) Test-case 3. (d) Test-case 4.

4.3.1 Stability Evaluation Criterion

Given a bounded region, the accuracy of IDM in terms of RMSE, maximum absolute intensity error, and maximum K-band line width, are analyzed for the final OPCed mask solution of a specific target pattern within this region. With replicating this target pattern among this bounded region to form target patterns with larger area/density, if IDM accuracy metrics keep almost the same values with this increased pattern area/density, this will confirm the stability of IDM.

4.3.2 Case of Study

Given the target pattern shown in Fig. 14 (a) in a 1236×885 pixels bounded region (the black area which is a sub-region from the total layout region in Lithosim), the pattern is repeated within this bounded region to generate test-cases with larger scales as illustrated in Fig. 14. OPC with IDM methodology is applied on each test-case to find its mask solution (shown in Fig. 15) with acceptable wafer images (shown in Fig. 16).

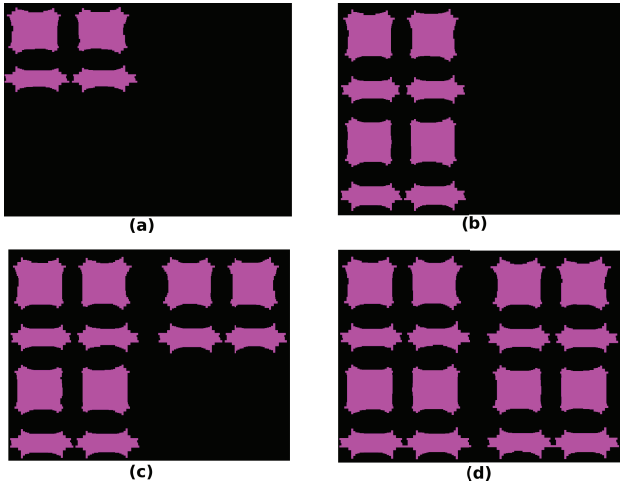
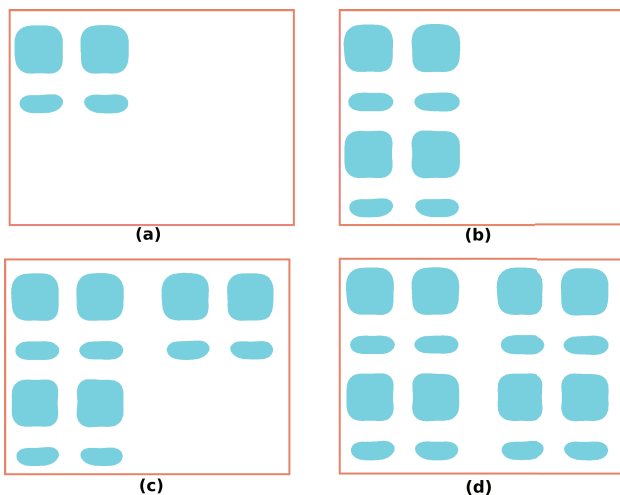
Note that replicating the target pattern does not mean replicating the mask solution. The reason is the existence of other polygons generated after replication that would impact the intensity of the other polygons nearby, and thus, the OPC response (shifting and hammering) is expected to be a bit different, specially for those polygons closed to the other replicated patterns.

For each test-case OPCed mask solution (outputted from the OPC algorithm), IRMSE, maximum absolute intensity error, and

Table 1 Evaluation of IDM Stability.

Test Case	Pattern Area (nm ²)	Layout Density	IRMSE	E_{\max}	Max K-band Line Width (nm)
Test-case1	108601	0.12	0.0069	0.0137	4
Test-case2	217201	0.21	0.0065	0.0125	4
Test-case3	325801	0.30	0.0066	0.0128	4
Test-case4	434401	0.40	0.0063	0.0126	4

Total region area: 1236 nm × 885 nm, $I_{\text{th}} = 0.225$, $EPE_{\max} = 15$ nm


Fig. 15 OPCed mask patterns for different area/density cases: (a) Test-case 1. (b) Test-case 2. (c) Test-case 3. (d) Test-case 4.

Fig. 16 Wafer images for different area/density cases through the OPCed masks: (a) Test-case 1. (b) Test-case 2. (c) Test-case 3. (d) Test-case 4.

maximum K-band line width are shown in **Table 1**. With increasing pattern area and density (from test-case 1 to test-case 4), maximum K-band line width remains the same (4 nm). IRMSE has 0.0006 maximum difference while the maximum absolute intensity error has 0.001 maximum difference. Wafer image computation is expected to be the same for all test-cases since the number of convolutions is the same. Notice that, IRMSE for test-case 4 is a bit less than that for test-case 1. A possible reason is that test-case 1 has fewer number of tap points. Thus, if a tap point deviation from the exact intensity is big, its impact on IRMSE value will be significant. On the other hand, test-case 4 has many tap points which makes such impacts on IRMSE less significant in total. Also, notice that E_{\max} for test-case 4 is less than that for test-case 1 as well. A possible reason is the exist-

tence of many tap points on the pattern boundary in test-case 1 which have the potential for bigger loss of accuracy. While, test-case 4 has many interior tap points whose intensity estimation error might be compensated with the intensity induced by the peripheral polygons nearby. However, this difference between the test-cases in IRMSE and E_{\max} is small and thus, can be affordable during intensity estimation.

As IDM methodology keeps almost the same wafer image accuracy metrics for different test-cases, this verifies its stability against pattern area/density increase. Thus, exploiting IDM in full chip OPC in the industry, is expected to significantly reduce the overall OPC computation time with preserving acceptable accuracy which turns out into outputting mask solutions with acceptable wafer image quality within a short time.

Finally, it is important to mention that we evaluated the proposed static IDM methodology using an industrial data. We implemented it to in-house OPC tool and carried out experimental comparison with using all kernels. We used a kind of industrial product data whose tile area is more than $10\mu\text{m} \times 10\mu\text{m}$. However, due to confidentiality, we cannot disclose details of that and the OPC tool. The experimental comparison was carried out on Linux OS, CPU: Xeon E5-2690 v2 (3.00 GHz), Memory: 256 GB with single processing. We confirmed that intensity difference map was 7.58X faster for aerial image calculation and 1.74X faster for OPC process than using all kernels at the cost of around 20% increase in the total EPE (average bit map difference between target pattern and obtained wafer image).

5. Adaptation of IDM

To improve the intensity estimation accuracy of IDM, adaptation of IDM has been proposed in our work in Refs. [11], [12]. The purpose of such adaptation is to improve the accuracy of IDM iteratively with considering the difference in local mask density between the mask of interest and the reference mask.

5.1 Adaptive IDM Methodology

A linearity has been observed between local mask density around a certain pixel (the ratio of mask pixels number intersecting the local region around a pixel to the total number of pixels in that local region as shown in **Fig. 17** (a)) and the intensity of that pixel using lower weight kernels. This linearity is exploited to adaptively improve the accuracy of IDM following mask shape changes from local density perspective.

Thus, the layout region is divided into grids as shown in **Fig. 17** (b). The linearity coefficient per grid is interpolated in the initialization phase of OPC. Thereafter, OPC is applied iteratively while those correction coefficients multiplied by the local mask density difference between the mask of interest and the reference mask (which has been chosen as the mask generated in

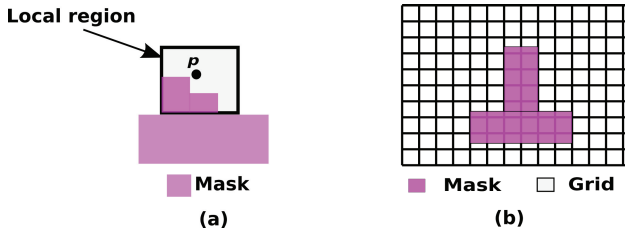


Fig. 17 (a) Local squared region around pixel p . The ratio of mask pixels intersecting this region represents the local mask density around pixel p . (b) Layout region gridding.

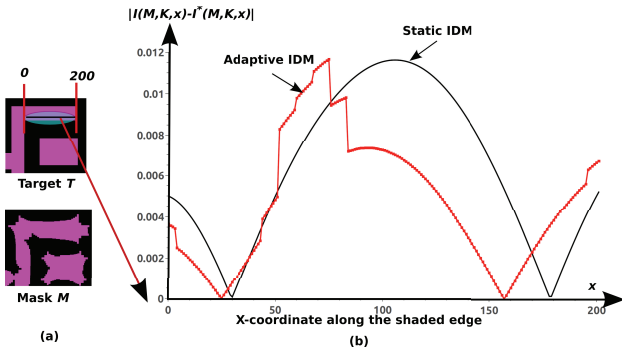


Fig. 18 (a) A portion of the target T and its OPCed mask M . (b) Absolute intensity error through mask M from the left corner to the right corner of the shaded edge in the target when the intensity is estimated using static IDM (black curve) and adaptive IDM (red curve).

the previous iteration) are included in intensity estimation per tap point, as given in Eq. (9), where $\Delta\delta(M, M_{\text{ref}}, w_i)$ denotes the local mask density difference between masks M and M_{ref} in grid w_i and $\gamma(w_i)$ is the linearity coefficient per grid w_i for which tap point t_i belongs [12].

$$I^*(M, K, t) |_{t \in w_i} = I(M, \{k_0\}, t) + I_{\text{diff}}(M_{\text{ref}}, K, \{k_0\}, t) + \gamma(w_i) * \Delta\delta(M, M_{\text{ref}}, w_i) \quad (9)$$

5.2 Case of Study

Figure 18 (a) illustrates a portion from a target pattern and its OPCed mask solution using adaptive IDM methodology. Figure 18 (b) illustrates absolute intensity error distribution through the OPCed mask in the pixels along the shaded edge in the target pattern from the left corner to the right corner. The intensity of this OPCed mask has been estimated using static IDM (black curve) and adaptive IDM (red curve). The grid size in this experiment has been chosen as 8×8 pixels. The improvement in estimation due to IDM adaptation is evident in most of the pixels. However, intensity estimation worsens a little bit in some pixels. Thus, more complicated models to extract the linearity coefficients might be required in the future for a better estimation with this adaptation methodology.

6. IDM Methodology Enhancement

Although the effectiveness of IDM and its adaptation in finding a mask solution under relaxed EPE constraint is evident, the loss of accuracy in intensity estimation at some regions might be problematic in twofolds: First of all, such loss of accuracy might not yield into proper mask solution if more strict EPE constraints are imposed. Secondly, some advanced technology nodes require very complicated resist models in both Positive Tone Develop-

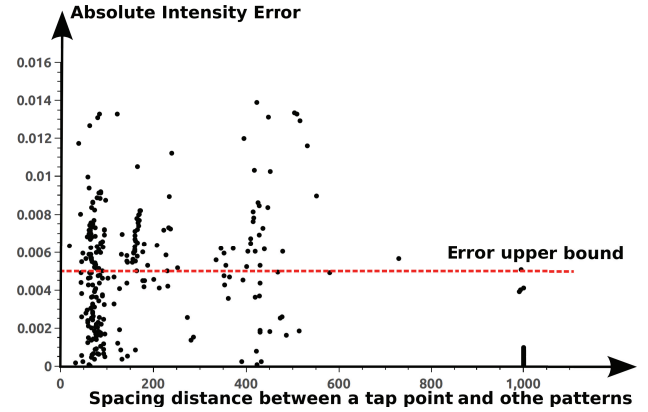


Fig. 19 Absolute intensity error for randomly chosen tap points versus the spacing distance between each tap point and other mask patterns. This data were extracted from the OPCed mask generated in Fig. 9 with static IDM for intensity estimation. $E_U = 0.005$ in this case.

ment (PTD) and Negative Tone Development (NTD), rather than CTR model. In such complicated models, any loss of accuracy in intensity estimation is accounting and impacts the quality of the OPC solution.

This section provides a formal definition for the lack of accuracy and proposes an analysis about the regions vulnerable to suffer from such accuracy loss in intensity estimation with IDM methodology. Thereafter, possible enhancements for the accuracy of IDM methodology are proposed.

6.1 Sources for Loss of Accuracy In Intensity Estimation

To formulate the lack of accuracy in intensity estimation, upper bound of the absolute intensity error is predefined. Let E_U denote this upper bound. The intensity of a tap point $t \in A$ is said to be accurately estimated if $|I(M, K, t) - I^*(M, K, t)| \leq E_U$, otherwise, the intensity of t is said to be suffering from lack of accuracy.

The existence of other polygons surrounding a tap point with small spacings has been found as a cardinal source for the loss of intensity estimation accuracy based on our observation. This is called the congestion of a tap point. That is, if a tap point is surrounded by other patterns with spacing distance between that tap point and the other polygons less than a certain threshold distance, that tap point intensity estimation accuracy is degraded. Such an observation is reasonable since light interference becomes pronounced in dense patterns.

Figure 19 illustrates the absolute intensity error for several tap points chosen from an OPCed mask estimated using static IDM versus the spacing distance between each tap point and other patterns in the mask. With strictly setting the upper bound of the absolute intensity error to 0.005, it is obvious in the plot that most of the tap points suffering from lack of accuracy ($E(M, t) > E_U$) are those with small spacing distance to other patterns.

Figure 20 illustrates an example showing the impact of neighboring patterns in the mask on intensity estimation. With going along the shaded edge from the left towards the right (where other patterns exist), absolute intensity error gradually increases and exceeds its upper bound at some point.

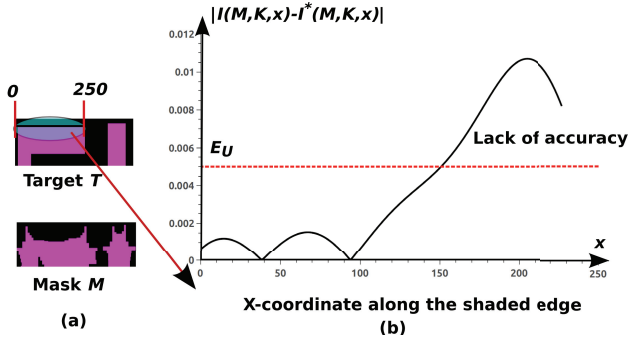


Fig. 20 (a) A portion of the target T and its OPCed mask M . (b) Absolute intensity error through mask M from the left corner to the right corner of the shaded edge in the target.

6.2 Suggestions for IDM Methodology Enhancements

6.2.1 Including More Top Weight Kernels in IDM

To improve estimation accuracy if the upper bound of absolute intensity error is strictly requested to be small, computation time reduction constraint can be slightly relaxed. This is satisfied through including the minimal number of higher weight kernels in IDM such that the maximum absolute error becomes less than E_U for all tap points. This optimization problem is formulated in Eq. (10) where $I_{\text{diff}}(M, K, K', t)$ is given in Eq. (3), M_{ref} is the chosen reference mask, $(I(M, K', t) + I_{\text{diff}}(M_{\text{ref}}, K, K', t))$ is the estimated intensity in tap point t , i.e., $I^*(M, K, t)$, and A denotes the set of tap points.

Choose minimal set $K' \subset K$

Subject to

$$\forall t \in A, |I(M, K, t) - \{I(M, K', t) + I_{\text{diff}}(M_{\text{ref}}, K, K', t)\}| \leq E_U \quad (10)$$

The optimization problem given in Eq. (10) is resolved in a pre-processing stage prior to OPC following the simulation environment with using some testing benchmarks. Algorithm 1 proposes a simple algorithm to solve this optimization problem. Given a target pattern T , one OPC step is applied to generate mask M_{ref} from which IDM is constructed between all kernels and only top weight kernel. An OPCed mask M is generated by applying one OPC step on M_{ref} . Starting with $K' = \{k_0\}$, both exact and estimated intensity maps of mask M are simulated. As long there exist tap points whose absolute error exceeds E_U , the next top weight kernel in K is included in K' to re-construct IDM. This iterative process continues till the required accuracy is satisfied. Note that $\#TV$ denotes the number of tap points whose absolute intensity error is greater than E_U , as given in Eq. (11)

$$\#TV(M) = |\{t \mid t \in A, E(M, K, t) > E_U\}| \quad (11)$$

With applying Algorithm 1 on Lithosim for some benchmarks, K' is found to be $\{k_0, k_1\}$ to satisfy the condition of intensity estimation accuracy with $E_U = 0.005$. **Figure 21** illustrates the improvement in intensity estimation caused by including kernel k_1 in IDM instead of using only k_0 as in the previous usage of static IDM at the cost of slight increase in computation time since two convolutions per OPC iteration are performed. Notice that absolute intensity error of some points exceeds E_U . The reason

Algorithm 1

```

 $K' \leftarrow \phi$  // initially empty
 $K \leftarrow \{k_0, k_1, k_2, \dots, k_n\}$  // All kernels
 $M_{\text{ref}} \leftarrow \text{applyOPC}(T, K)$ 
 $\#EUV \leftarrow \infty$ 
 $M \leftarrow \text{applyOPC}(M_{\text{ref}}, K)$ 
 $i \leftarrow 0$ 
while  $\#EUV > 0$  OR  $|K'| == 0$  do
     $K' \leftarrow K' \cup \{k_i\}$ 
     $I(M) \leftarrow \text{simulateIntensityMap}(M, K)$ 
     $I_{\text{diff}}(M, K, K') \leftarrow \text{findIDM}(M_{\text{ref}}, K, K')$ 
     $I^*(M) \leftarrow \text{simulateIntensityMap}(M, K') + I_{\text{diff}}(M, K, K')$ 
     $\#TV \leftarrow \text{findNumberOfAccuracyLoss}(I(M), I^*(M), T, E_U)$ 
     $i \leftarrow i + 1$ 
end while
    
```

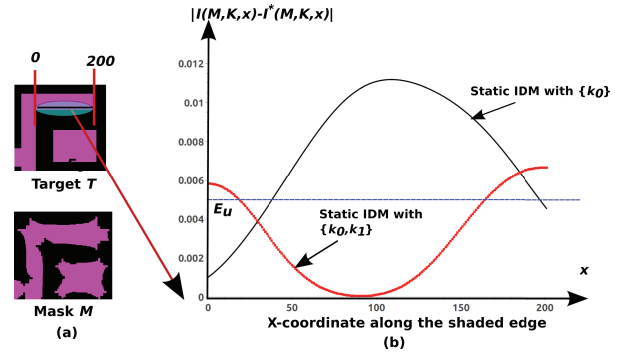


Fig. 21 (a) A portion of the target T and its OPCed mask M obtained using static IDM methodology. (b) Absolute intensity error through mask M from the left corner to the right corner of the shaded edge in the target when the intensity is estimated using static IDM with only top weight kernel (black curve) and static IDM with first two top weight kernels (red curve). E_U in this example is 0.005.

is that our formulated optimization problem in Eq. (10) considers making the intensity error of each tap point less than E_U , while the curve shows the intensity error for each pixel along the shaded edge. Additionally, this lack of estimation accuracy is basically observed near the corners whose intensity estimation requires more complicated models due to the typical lack/excess of intensity there. However, such lack of estimation around the corners can be affordable under relaxed EPE constraints, as long as no electric violations occur.

Computation time is proportional to the number of convolutions during each OPC iteration. Thus, the increased amount in computation time, which is resultant from relaxing time constraint, is correlated to the additional number of kernels by which the mask is iteratively convolved. Let τ denote the computation time required to compute the wafer image in some OPC iteration, and let K' denote the set of higher kernels included in IDM (used in Eq. (10)). Let τ_s denote the computation time that one convolution operation costs. With our original IDM methodology (using only top weight kernel for compensation), $\tau = \tau_s$. However, with slightly relaxing time constraint, the computation time will increase by $\tau_s \times (|K'| - 1)$.

The maximum observed intensity error among tap points (E_{max}) decays with the increased number of the kernels included iteratively in simulation within our IDM methodology. This is reasonable since the more kernels, the more estimation accuracy,

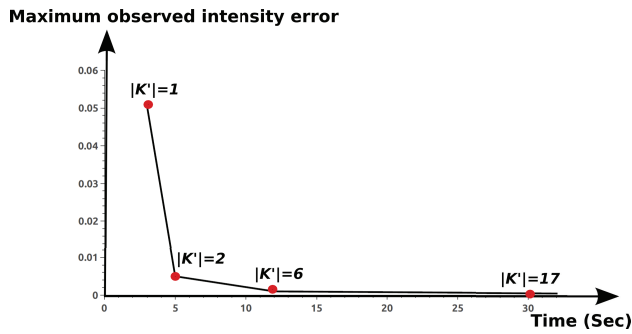


Fig. 22 Wafer image computation time versus maximum observed intensity error E_{\max} . Notice that less E_{\max} means the ability to utilize lower upper bound of the intensity error E_U at the cost of computation time increase. K' represents the set kernels found after solving the optimization problem given in Eq. (10).

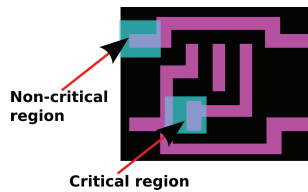


Fig. 23 Regions classification to critical and non-critical following the congestion nearby.

and thus, lower E_{\max} value. Consequently, utilizing low E_U (upper bound error) means longer computation time. The relation between E_{\max} and wafer image computation time τ is mathematically reasoned as given in Eq. (12). **Figure 22** illustrates a plot for wafer image computation time for the mask solution shown in Fig. 7 (a) versus the maximum observed intensity error. This plot shows E_{\max} decays with increasing computation time as a result of increasing the number of kernels needed. When E_{\max} reaches zero, this means all kernels are included in intensity estimation, and thus, maximizing wafer image computation time.

$$E_{\max} \propto \frac{1}{|K'|} \quad (12)$$

$$\tau \propto |K'| \implies E_{\max} \propto \frac{1}{\tau}$$

6.3 Sub-regions Intensity Estimation

Another enhancement without significant computation overhead is to divide the layout region into sub-regions and classify them following the distribution of absolute intensity error. If a region contains tap points whose absolute intensity error exceeds the upper bound of that error, the region is tagged as critical. Otherwise, it is non-critical. The intensity map of critical regions is simulated using more kernels while non-critical regions intensity maps are roughly estimated using static/adaptive IDM methodology. Although including more kernels entails increasing the convolution number, such convolutions will be applied on sub-regions which is less computationally expensive than the entire region convolution.

As explained in Section 6.1, if the spacing between a tap point and other patterns is less than a certain threshold distance, its region can be speculated as a critical region, and thus, simulated with more kernels. Such speculation reduces the time required to classify the regions using several simulations. **Figure 23** illus-

trates an example of regions classification following such speculation.

7. Concluding Remarks and Future Work

The effectiveness of Intensity Difference Map (IDM) in terms of accounting for the loss of accuracy and shortening computation time has been verified. With plotting the root mean square error, minimal and maximal absolute errors, and maximal kernel band line width, between exact and estimated wafer images, it has been proven that IDM iteratively minimizes those loss of accuracy metrics within a short computation time.

The stability of IDM has been verified through investigating the variations of accuracy metrics with increasing the area/density of the target pattern in the layout region. Experimental results show that accuracy metrics remain almost the same, which ensures IDM stability, and thus, its predicted effectiveness for full chip OPC.

Adaptation of IDM has been analyzed as well to verify the improvement in intensity estimation resultant from compensating static IDM with the local mask density difference between the mask of interest and the reference mask.

Finally, a deep analysis for the sources of loss of accuracy has been performed. The congestion of patterns has been found as a dominant factor in degrading IDM accuracy in some regions. Accordingly, several approaches have been proposed to improve the accuracy of estimation with IDM methodology. Including more top weight kernels in IDM increases its accuracy with a bit increase in computation time. This has been formulated in an optimization problem to be solved in an early preprocessing stage, such that the required accuracy criterion is satisfied, with adding the minimal number of top weight kernels in IDM. Estimating the intensity of what is tagged as critical sub-regions in the layout using more kernels has been suggested as well.

Overall, this paper verified the effectiveness of IDM methodology and proposed some enhancements for its future use. IDM has been found as a motivating methodology to shorten the computation time for recent aggressive OPC algorithms for advanced technology nodes with preserving an algorithm effectiveness in terms of wafer image quality.

Future work of this paper includes effective implementation of the suggested enhancements of IDM. Moreover, considering more complicated resist models and process variations for IDM form key concerns to be tackled as well in the future.

Acknowledgments This work was supported by JSPS KAKENHI Grant-in-Aid for Scientific Research (B)25280013.

References

- [1] Ma, X. and Arce, G.: *Computational Lithography*, Wiley Publisher (2010).
- [2] Fabian Pease, R. and Chou, S.: *Lithography and Other Patterning Techniques for Future Electronics*, *Proc. IEEE*, pp.248–270 (2008).
- [3] Granik, Y. and Cobb, N.: *Matrix Optical Process Correction*, US Patent US6928634 B2 (2003).
- [4] Gu, A. and Zakhor, A.: *Optical Proximity Correction With Linear Regression*, *IEEE Trans. Semiconductor Manufacturing*, pp.263–271 (2008).
- [5] Mukhejee, M., Buamm, Z., Lavin, M., Samuels, D. and Singh, R.: *Method for Adaptive Segment Refinement Optical Proximity Correction*, US Patent 7043712 (2006).

- [6] Cobb, N., Grodd, L., Lippincott, G. and Sahouria, E.: Selective promotion for resolution enhancement techniques, US Patent US20040230936 A1 (2004).
- [7] Su, Y.-H., Huang, Y.-C., Tsai, L.-C., Chang, Y.-W. and Banerjee, S.: Fast Lithographic Mask Optimization Considering Process Variation, *IEEE Trans. Computer Aided Design of Integrated Circuits and Systems* (2016).
- [8] Yu, P. and Pan, D.: A Novel Intensity Based Optical Proximity Correction Algorithm with Speedup in Lithography Simulation, *Proc. ICCAD*, pp.854–858 (2007).
- [9] Awad, A., Takahashi, A., Tanaka, S. and Kodama, C.: A Fast Process Variation and Pattern Fidelity Aware Mask Optimization Algorithm, *Proc. ICCAD*, pp.238–245 (2014).
- [10] Awad, A., Takahashi, A., Tanaka, S. and Kodama, C.: A Fast Process Variation Aware Mask Optimization Algorithm With A Novel Intensity Modeling, *IEEE Trans. Very Large Scale Integration Systems* (2017).
- [11] Awad, A., Takahashi, A. and Kodama, C.: A Fast Manufacturability Aware Optical Proximity Correction (OPC) Algorithm with Adaptive Wafer Image Estimation, *Proc. DATE*, pp.49–54. (2016).
- [12] Awad, A., Takahashi, A. and Kodama, C.: A Fast Manufacturability and Process Variation Aware OPC Algorithm With Exploiting A Novel Intensity Estimation Model, *IEICE Trans. Fundamentals of Electronics, Communications and Computer Sciences*, Vol.E99-A, No.12, pp.2363–2374 (2016).
- [13] Leibman, L., Bruce, J., Chu, W., Cross, M., Graur, I., Krueger, J., Leipold, W., Mansfield, S., McGuire, A. and Sundlig, D.: Optimizing Style Options for Sub-Resolution Assist Features, *Proc. SPIE 4346, Optical Microlithography XIV* (2001).
- [14] Mansfield, S., Leibman, L., Molless, A. and Wong, A.: Lithographic Comparison of Assist Features Design Strategies, *Proc. SPIE*, Vol.4346 (2000).
- [15] Hamouda, A., Anis, M. and Karim, K.: Using Segmented Models for Initial Mask Perturbation and OPC Speedup, *Proc. SPIE 8880, Photomask Technology* (2013).
- [16] Lei, J., Hong, L., Lippincott, G. and Word, J.: Model-based OPC using MEEF matrix II, *Proc. SPIE 9052, Optical Microlithography XXVII* (2014).
- [17] Awad, A. and Takahashi, A.: A Lithographic Mask Manufacturability and Pattern Fidelity Aware OPC Algorithm, *Proc. International Symposium on VLSI Design, Automation and Test (VLSI-DAT)*, pp.D3-7-1-4 (2016).
- [18] Pang, L., Liu, Y. and Abrams, D.: Inverse Lithography Technology (ILT), What is the Impact to Photomask Industry?, *Proc. SPIE 6283, Photomask and Next-Generation Lithography Mask Technology XIII, 62830X* (2006).
- [19] Yu, P. and Pan, D.: TIP-OPC: A New Topological Invariant Paradigm for Pixel Based Optical Proximity Correction, *Proc. ICCAD*, pp.847–853 (2007).
- [20] Shiori, S. and Tanabe, H.: Fast Optical Proximity Correction: Analytical Method, *Proc. SPIE 2440*, pp.261–269 (1995).
- [21] Gallatin, G., Lai, K., Mukhejee, M. and Rosenbluth, A.: Printability Verification By Progressive Modeling Accuracy, US Patent 7512927 (2009).
- [22] Gao, J., Xu, X., Yu, B. and Pan, D.: MOSAIC: Mask Optimization Solution With Process Window Aware Inverse Correction, *Proc. DAC*, pp.1–6 (2014).
- [23] Cobb, N.: Sum of Coherent Systems Decomposition by SVD, Berkeley CA 94720, pp.1–7 (1995).
- [24] Kumar, P., Barai, S., Srinivasan, B. and Mohapatra, N.: Process Model Accuracy Enhancement Using Cluster Based Approach, *17th International Workshop on the Physics of Semiconductor Devices*, pp.33–36 (2013).
- [25] Sturtevant, J.: Challenges for Patterning Process Models Applied to Large Scale, *Journal of Vacuum Science & Technology*, pp.1–10 (2012).
- [26] Satake, M.: Lithography simulation method, method of manufacturing a semiconductor device and program, U.S. Patent 7870532 (2011).
- [27] Randall, J., Gangala, H. and Tritchkov, A.: Lithography simulation with aerial image – Variable threshold resist model, *International Conference on Micro- and Nanofabrication*, pp.59–63 (1999).
- [28] Banerjee, S., Li, Z. and Nassif, S.: ICCAD-2013 CAD Contest in Mask Optimization and Benchmark Suite, *Proc. ICCAD*, pp.271–274 (2013).



Ahmed Awad received his Bachelor and master degrees from the department of computer systems engineering, Birzeit university, Palestine, in 2009 and 2011, respectively. He worked as a quality assurance engineer for CISCO systems from 2010-2013. He is currently pursuing his PhD degree in the department of communications and computer engineering in Tokyo Institute of Technology, Japan. His research interests include VLSI physical design, OPC, and low power VLSI testing.



Atsushi Takahashi received his B.E., M.E., and D.E. degrees in electrical and electronic engineering from Tokyo Institute of Technology, Tokyo, Japan, in 1989, 1991, and 1996, respectively. He had been with the Tokyo Institute of Technology as a research associate from 1991 to 1997, and as an associate professor from 1997 to 2009 and from 2012 to 2015, and as a professor from 2015. He had been with the Osaka University as an associate professor from 2009 to 2012. He is currently with Department of Information and Communications Engineering, School of Engineering, Tokyo Institute of Technology. He is currently a member of IEEE Circuits and Systems Society Board of Governors (BoG) and the chair of CEDA All Japan Joint Chapter. His research interests are in VLSI layout design and combinational algorithms. He is a senior member of IEEE, IEICE and IPSJ, and a member of ACM.



Satoshi Tanaka received his MS in nuclear engineering from The University of Tokyo in 1992, and joined ULSI Research Center of Toshiba Corporation. He had engaged in research and development of optical lithography simulation field, and current his interest includes computational lithography.



Chikaaki Kodama received his B.E., M.E., and D.E. degrees in electronic and information engineering from Tokyo University of Agriculture and Technology, Tokyo Japan, in 1999, 2001, and 2006, respectively. He is currently with Toshiba Corporation. He is a senior member of IEEE and IEICE.

(Recommended by Associate Editor: Makoto Sugihara)